Supplementary Information

Carboxylate-functionalized polymers of intrinsic microporosity for High-Performance Osmotic Power Conversion

Changhao Li [a], Xianxian Mei [a], Hanwen Yang [a], Minghui Cheng [a], Xin Zhou [a], Zipei Zhang [a], Mi Lu [a], Jianping Lin [a,*]

[a] School of Materials Science and Engineering, Xiamen University of Technology, Xiamen, 361024, PR China

* Corresponding author. Email address: jplin@xmut.edu.cn

Supplementary Notes

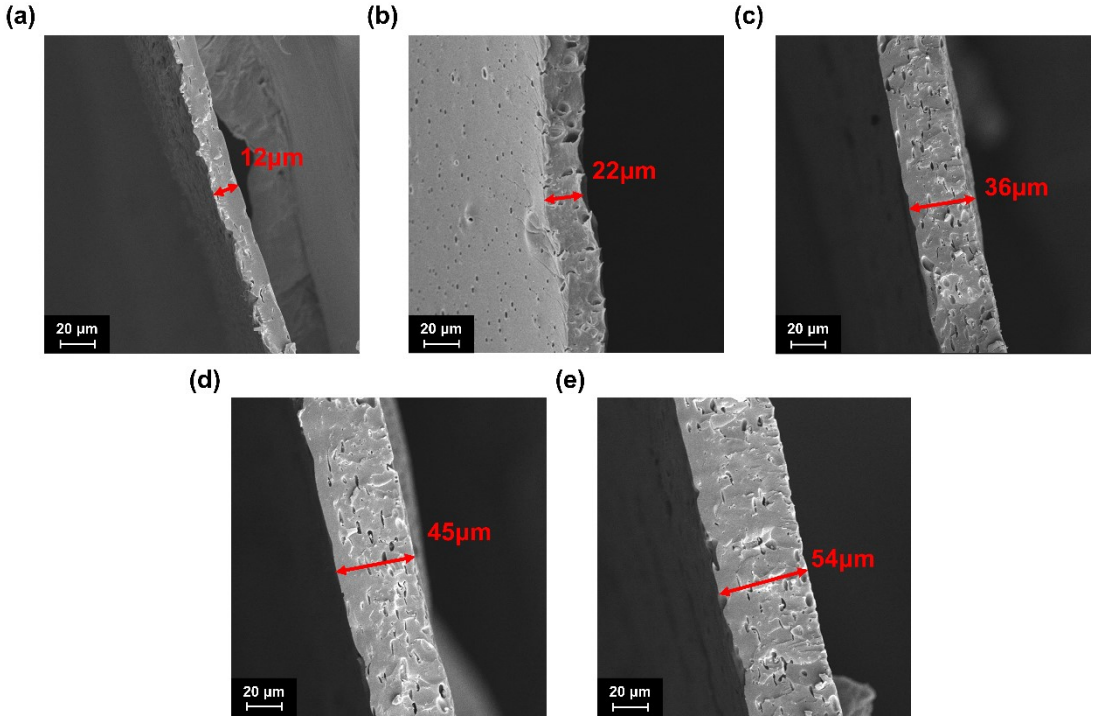

Fig. S1. SEM cross-sectional images of PIM-1-COONa films with different thicknesses.

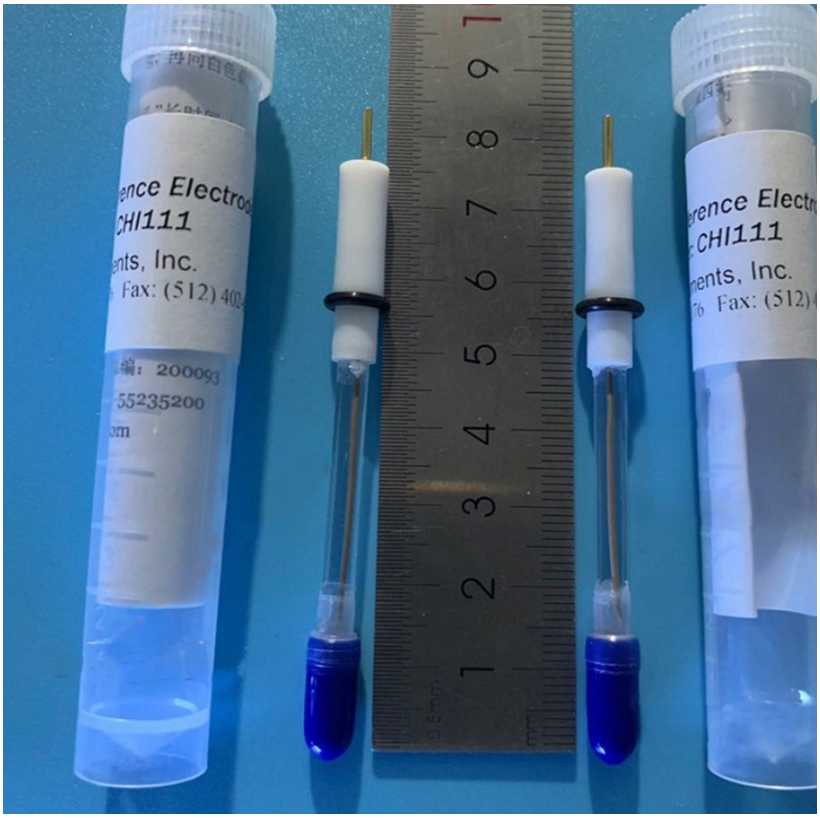

Fig. S2. A picture of the commercially available standard Ag/AgCl electrodes used in the experiment. The electrodes should be removed and rinsed with deionized water when used for measurements in the osmotic power conversion experiment.

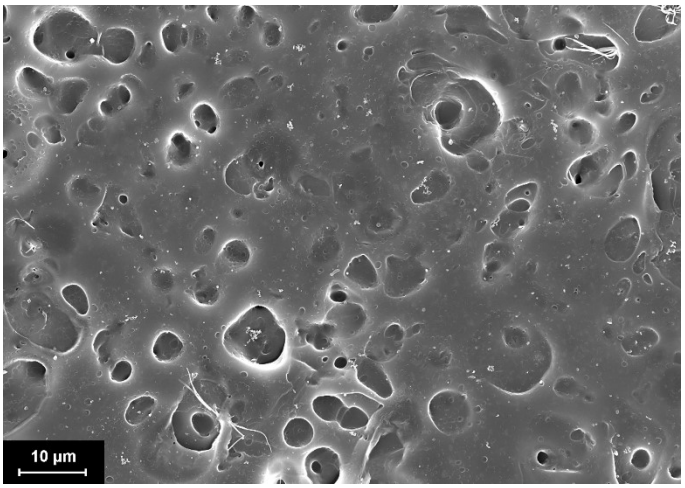

Fig. S3. SEM image of the PIM-1-COONa membrane treated with alkaline hydrolysis for 8 hours.

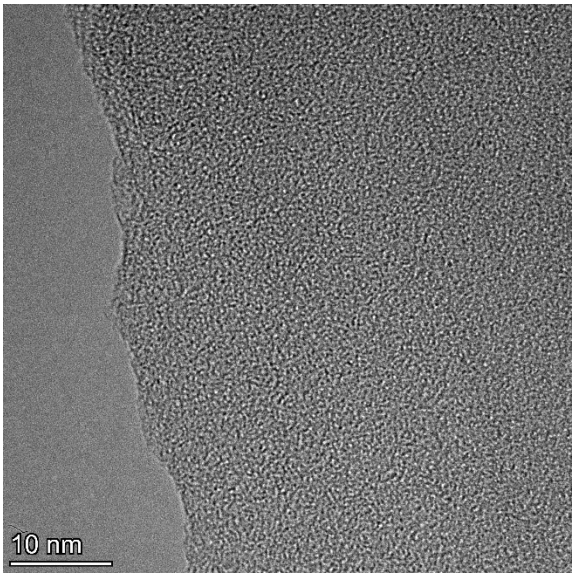

Fig. S4. HRTEM image of the PIM-1-COONa membrane

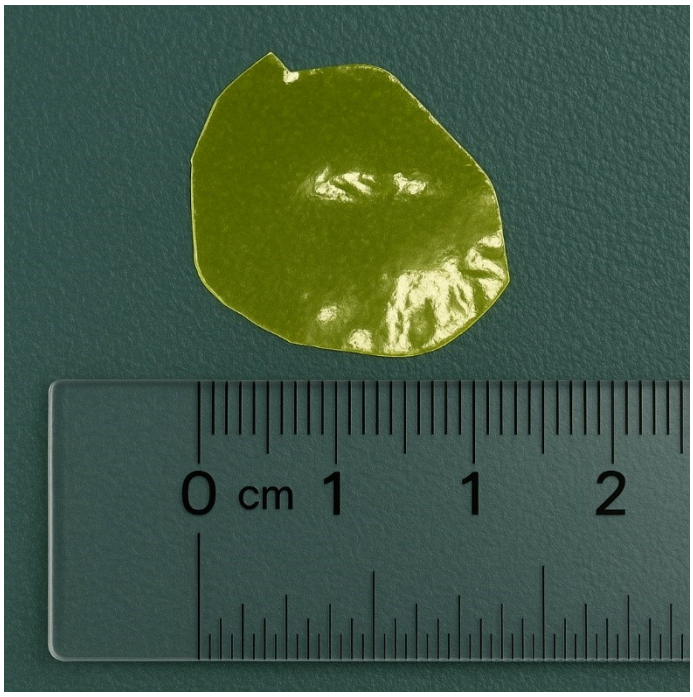

Fig. S5. Photograph of the pristine PIM-1 membrane.

Fig. S6. Photograph of the PIM-1-COONa (30 μm) film.

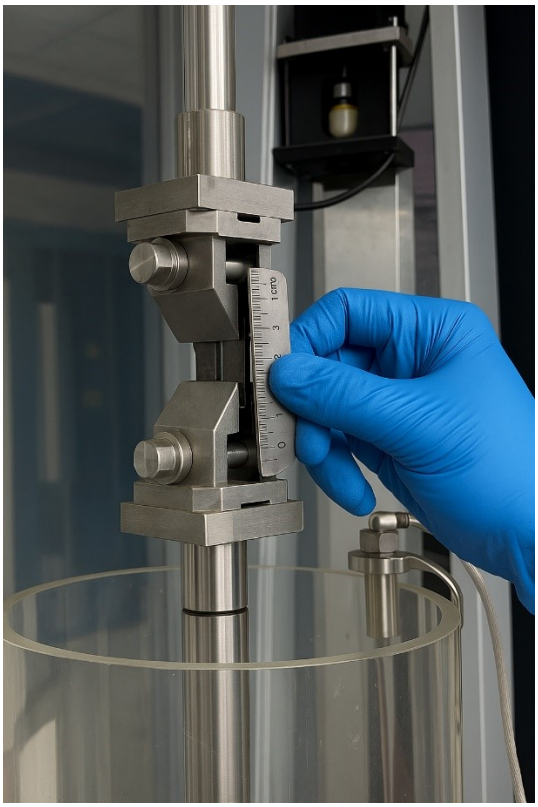

Fig. S7. Mechanical testing machine used for measuring the mechanical properties of the PIM-1-COONa membrane.

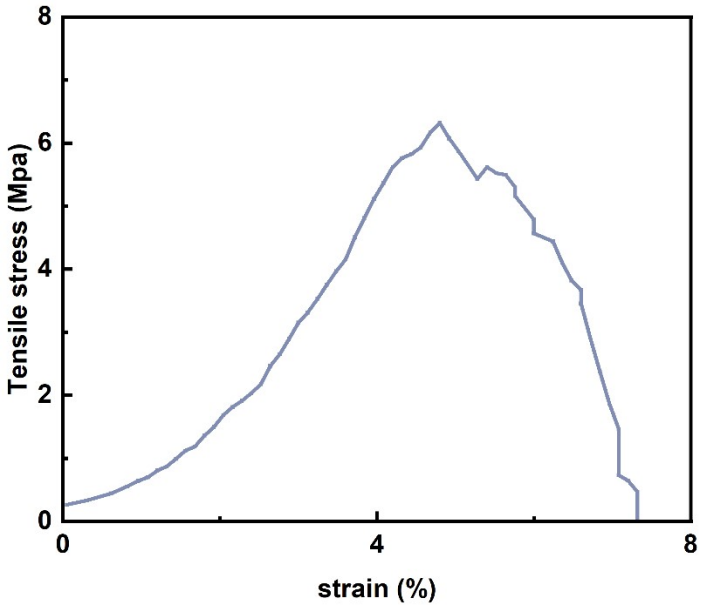

Fig. S8. Tensile stress-strain curve of the PIM-1-COONa membrane.

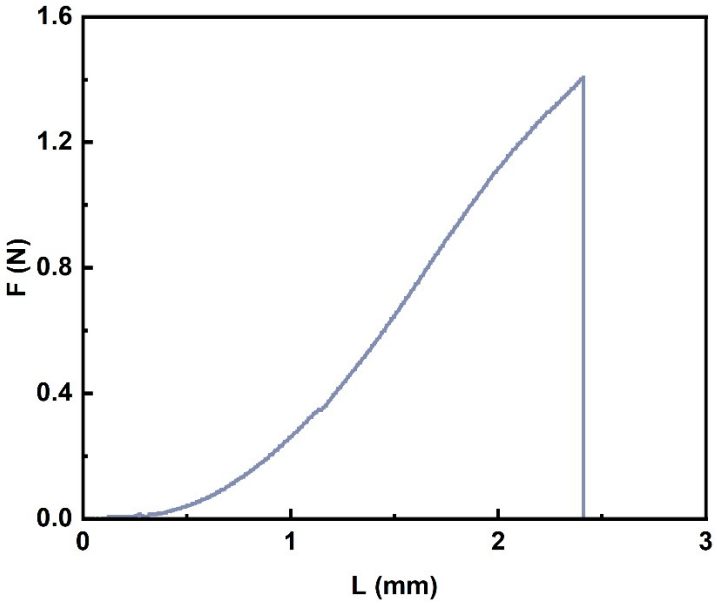

Fig. S9. Puncture force-deformation curve of the PIM-1-COONa membrane.

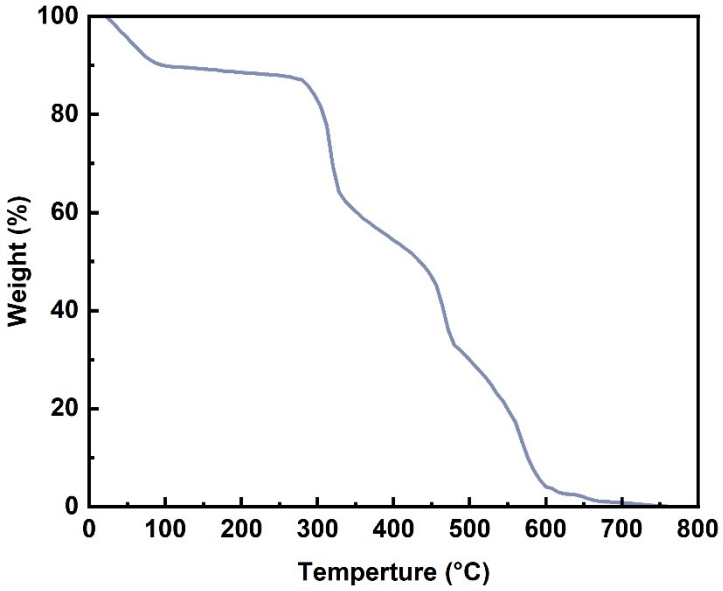

Fig. S10. Thermogravimetric analysis of the PIM-1-COONa membrane under air atmosphere.

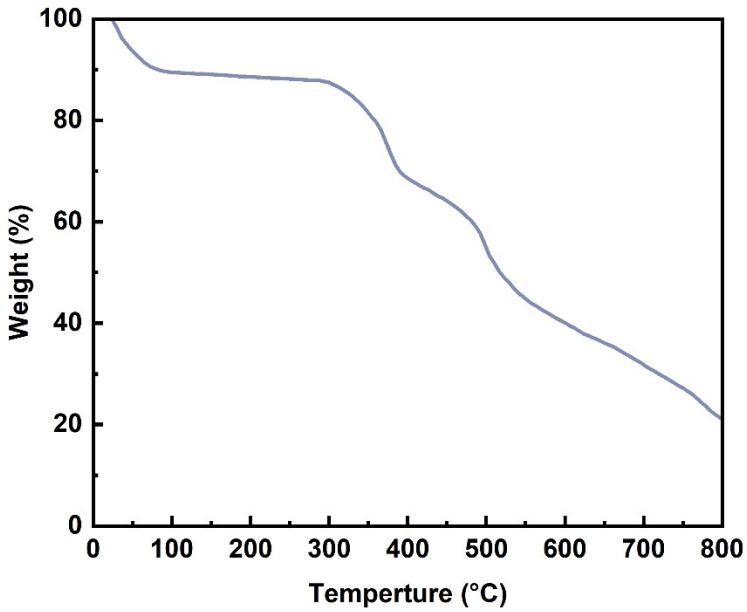

Fig. S11. Thermogravimetric analysis of the PIM-1-COONa membrane under nitrogen atmosphere.

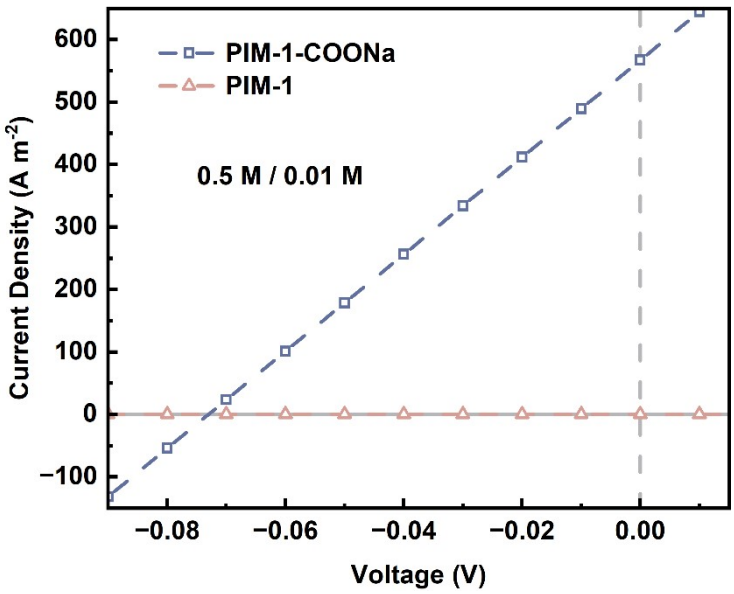

Fig. S12. Comparison of current density-voltage (J-V) characteristics for the PIM-1 membrane and the PIM-1-COONa membrane.

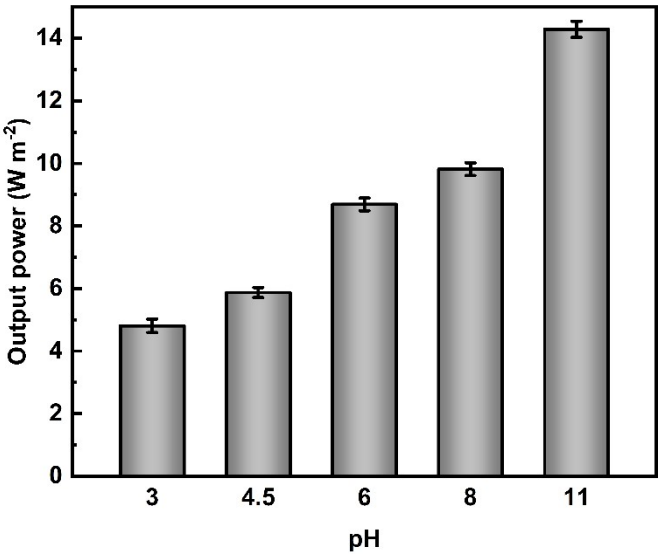

Fig. S13. Output power of the membrane under different pH conditions.

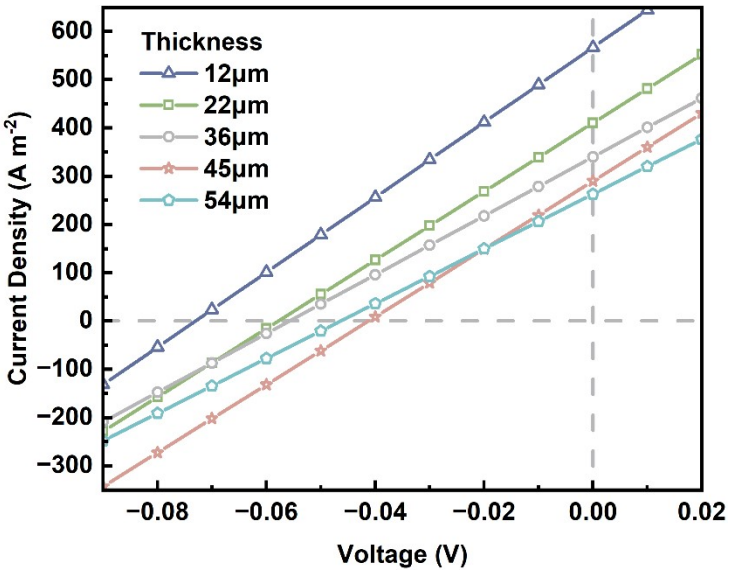

Fig. S14. Comparison of current density-voltage (J-V) characteristics for PIM-1-COONa membranes with different thicknesses.

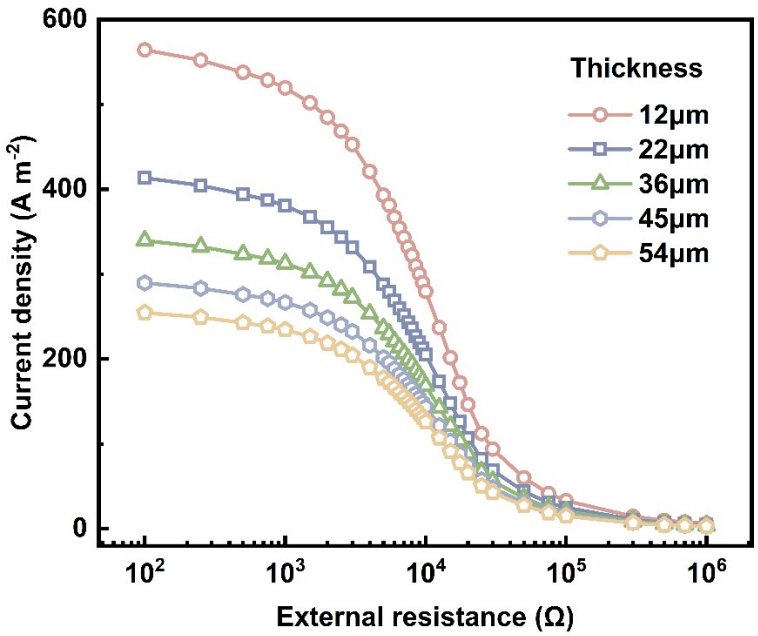

Fig. S15. Current density of PIM-1-COONa under different external resistances at different thicknesses.

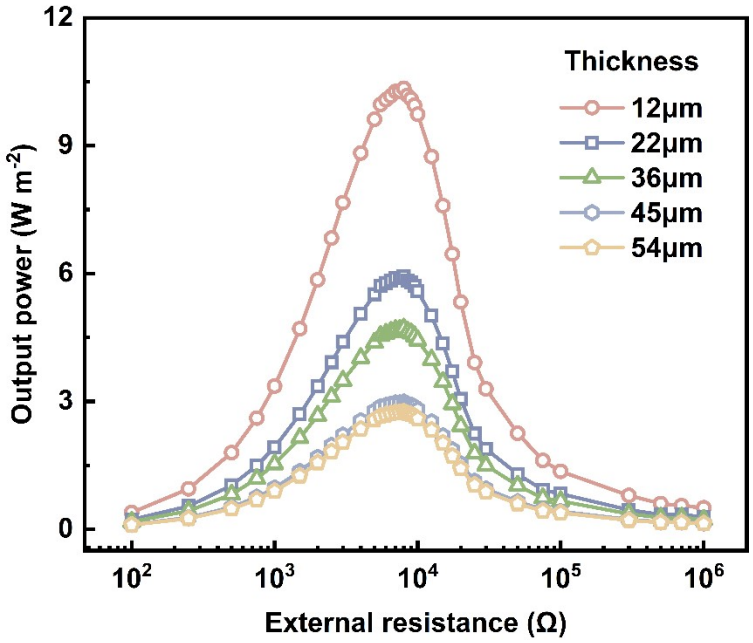

Fig. S16. Power density of PIM-1-COONa under different external resistances at different thicknesses.

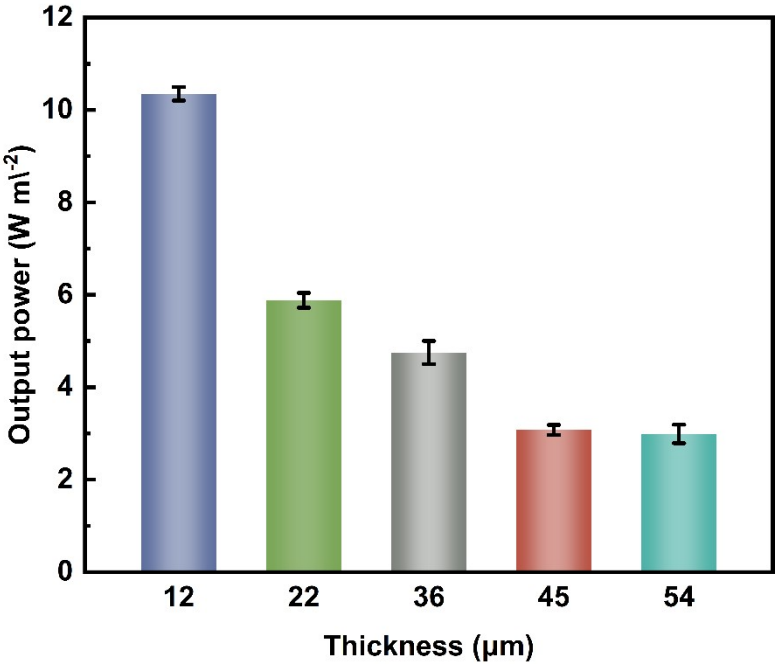

Fig. S17. Comparison of maximum output power densities for PIM-1-COONa membranes with different thicknesses.

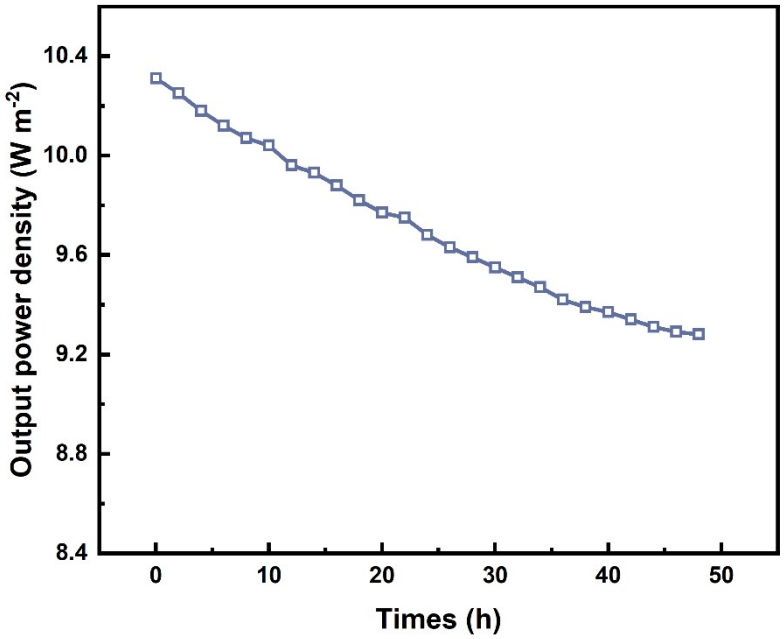

Fig. S18. The maximum osmotic power output of the PIM-1-COONa membrane remained above 90% of its initial value over 48 hours.

Supplementary Table 1. Open-circuit voltage (V_{oc}), short-circuit current (I_{sc}), short-circuit current density (J), and maximum output power density (P_{max}) for PIM-1-COONa membranes of different thicknesses under a 50-fold concentration gradient.

Thickness (μm)	V_{oc} (mV)	I_{sc} (μA)	J (A m^{-2})	P_{max} (W m^{-2})
12	73.04	17	566.67	10.34
22	57.78	12.33	411	5.94
36	55.72	10.19	339	4.72
45	41.21	8.69	290	2.99
54	43.31	7.69	256.3	2.77

Supplementary Table 2. Energy conversion performance across different membranes under simulated seawater and river water conditions. V_{oc}, I_{sc}, and P_{max} represent the membrane potential, ionic current, and maximum output power density, respectively.

Material system	V_{oc} (mV)	I_{sc} (A m^{-2})	P_{max} (W m^{-2})	Thickness (μm)	Ref.
This work	73.04	566.67	10.34	12	-
J-MOF	163.1	84.41	3.44	1	[1]
PSS/MOF	70	170	2.87	1.6	[2]
ZnTCPP/MOF	93	129.03	3	4	[3]
SPEEK/SPSF	140	200	7	4	[4]
COF-LZU1@CNT-CNF	39	436.92	4.26	0.47	[5]
WO_3-AAO-ZIF-8	71	108.73	1.93	4.2	[6]
TpPa-SO_3H	115	205.22	5.9	10.7	[7]
MOF-on-MOF	75	465.07	8.72	75.7	[8]
SPIM	76	504.21	9.58	108	[9]

Reference

1 Z.-Q. Li, G.-L. Zhu, R.-J. Mo, M.-Y. Wu, X.-L. Ding, L.-Q. Huang, Z.-Q. Wu and X.-H. Xia, *ACS Appl. Mater. Interfaces*, 2023, **15**, 23922–23930.

2 R. Li, J. Jiang, Q. Liu, Z. Xie and J. Zhai, *Nano Energy*, 2018, **53**, 643–649.

3 Y. Su, J. Hou, C. Zhao, Q. Han, J. Hu and H. Zhang, *J. Mater. Chem. A*, 2024, **12**, 13153–13159.

4 X. Zhao, C. Lu, L. Yang, W. Chen, W. Xin, X.-Y. Kong, Q. Fu, L. Wen, G. Qiao and L. Jiang, *Nano Energy*, 2021, **81**, 105657.

5 R. Li, J. Zhai, J. Jiang, Q. Wang and S. Wang, *ACS Appl. Energy Mater.*, 2022, **5**, 7176–7184.

6 L. Fu, Y. Wang, J. Jiang, B. Lu and J. Zhai, *ACS Appl. Mater. Interfaces*, 2021, **13**, 35197–35206.

7 S. Hou, W. Ji, J. Chen, Y. Teng, L. Wen and L. Jiang, *Angew. Chem. Int. Ed.*, 2021, **60**, 9925–9930.

8 R. K. Tonnah, M. Chai, M. Abdollahzadeh, H. Xiao, M. Mohammad, E. Hosseini, M. Zakertabrizi, D. Jarrahbashi, A. Asadi, A. Razmjou and M. Asadnia, *ACS Nano*, 2023, **17**, 12445–12457.

9 S. Zhou, X. Lin, Y. Hu, L. Fu, Q. Luo, L. Yang, S. Hou, X.-Y. Kong, L. Jiang and L. Wen, *ACS Mater. Lett.*, 2022, **4**, 1422–1429.